Wrecking neutrophil extracellular traps and antagonizing cancer-associated neurotransmitters by interpenetrating network hydrogels prevent postsurgical cancer relapse and metastases☆

Hang Zhou [a],[1], Chunyan Zhu [b],[c],[1], Qing Zhao [a],[1], Jinliang Ni [b],[c], Haipeng Zhang [b],[c], Guangcan Yang [b],[c], Jianchao Ge [b], Chao Fang [b], Hong Wei [a], Xianli Zhou [a],[**], Kun Zhang [b],[c],[*]

[a] In-Patient Ultrasound Department, Second Affiliated Hospital of Harbin Medical University, Surgeons' Hall, No.246. XuefuRoad, Nangang District, Harbin City, Heilongjiang Prov, PR China
[b] Department of Laboratory Medicine and Central Laboratory, Sichuan Academy of Medical Sciences, Sichuan Provincial People's Hospital, School of Medicine, University of Electronic Science and Technology of China, No. 32, West Second Section, First Ring Road, Chengdu, 610072, Sichuan, PR China
[c] Ultrasound Research and Education Institute, Shanghai Tenth People's Hospital, Tongji University School of Medicine, No. 301 Yan-chang-zhong Road, Shanghai, 200072, PR China

ARTICLE INFO

ABSTRACT

Tumor-promoting niche after incomplete surgery resection (SR) can lead to more aggressive local progression and distant metastasis with augmented angiogenesis-immunosuppressive tumor microenvironment (TME). Herein, elevated neutrophil extracellular traps (NETs) and cancer-associated neurotransmitters (CANTs, e.g., catecholamines) are firstly identified as two of the dominant inducements. Further, an injectable fibrin-alginate hydrogel with high tissue adhesion has been constructed to specifically co-deliver NETs inhibitor (DNase I)-encapsulated PLGA nanoparticles and an unselective β-adrenergic receptor blocker (propranolol). The two components (i.e., fibrin and alginate) can respond to two triggers (thrombin and Ca^{2+}, respectively) in post-operative bleeding to gelate, shaping into an interpenetrating network (IPN) featuring high strength. The continuous release of DNase I and PR can wreck NETs and antagonize catecholamines to decrease microvessel density, blockade myeloid-derived suppressor cells, secrete various proinflammatory cytokines, potentiate natural killer cell function and hamper cytotoxic T cell exhaustion. The reprogrammed TME significantly suppress locally residual and distant tumors, induce strong immune memory effects and thus inhibit lung metastasis. Thus, targetedly degrading NETs and blocking CANTs enabled by this in-situ IPN-based hydrogel drug depot provides a simple and efficient approach against SR-induced cancer recurrence and metastasis.

01. Introduction

Surgical resection (SR) is the primary treatment for most early-stage solid tumors [1], whereas postoperative relapse and metastases pose major challenge to patients' overall survival [2]. It has been well-recognized that the locally-persisting and minimal residual niche after resection may undergo biological perturbations associated with the surgical stress response and escape equilibrium to promote disease progression [3]. Therefore, screening and targeting the determinant signaling pathways that involve the activation of physiological responses to surgery is beneficial for designing drugs or technologies to suppress tumor relapse, and improve patient prognosis [3].

Cancer extracellular matrix (ECM) or microenvironment reprogramming after SR have been demonstrated to correlate with tumor relapse and metastasis and resist auxiliary chemotherapy or immunotherapy [4–6], which give us a distinctive inspiration source.

Neutrophils are firstly recruited and arrive at the site of surgical bed after tissue damage. Due to the damages-associated molecular patterns (DAMPs) release during surgery, neutrophils undergo a programmed cell death to combat certain infections (NETosis), wherein neutrophil extracellular traps (NETs) featuring web-like structures composing of DNA, histones, and antimicrobial proteins were shaped to kill pathogens [7]. Increasing evidences suggest that NETs play a critical role in accelerating tumor growth by inhibiting function of natural killer (NK) and T cell [8,9], awakening dormant cancer cells [10], and shielding them against immune cell-mediated killing effect [11]. Apart from NETs, surgical procedures-related pain, anxiety and wound injury may also activate adrenergic nerve signaling, triggering excessive perioperative secretion of neurotransmitters, such as catecholamines [12]. Through binding to adrenergic G protein-coupled receptors (GPCRs), catecholamines may serve as cancer-associated stress hormone to augment the infiltrated pro-tumorigenic myeloid-derived suppressor cells (MDSCs) [13,14], which can dampen the activity of both adaptive and innate immune system [15]. Furthermore, catecholamines could significantly promote the expression of angiogenic factors including vascular endothelial growth factor (VEGF) and aggravate tumor microvascularization [16].

Taken above together, NETs and cancer-associated neurotransmitters (CANTs) are anticipated to be two targets associated with postsurgical tumor relapse and metastasis. To ascertain them, a preclinical surgery resection (SR) model was established in this report, where the elevated NETs and CANTs (e.g., catecholamines) were identified as one of the main factors in augmenting angiogenesis-encouraged immunosuppressive tumor microenvironment (TME). Inspiringly, the two definite targets were further harnessed to design and engineer an injectable and interpenetrating network (IPN)-structured hydrogel as a drug depot to targetedly degrade NETs and blockade catecholamines for repressing cancer relapse and metastasis. Herein, unselective beta-adrenergic receptor blocker, propranolol (PR) and poly (lactic-co-glycolic acid) (PLGA) nanoparticles loaded with NETs inhibitor DNase I were encapsulated in such injectable IPN-structured hydrogels consisting of fibrin and alginate (PR@DNase I-PLGA@Gel) (Fig. 1). Fibrin is involved in the coagulation cascade, forming a physiologic clot framework in response to thrombin. Alginate can respond to Ca^{2+} and gelate into another framework that unite with fibrin gelation framework to shape into the IPN structure. The two components are biocompatible and will not cause inflammation, tissue necrosis, or fibrosis, and different biological triggers (thrombin, Ca^{2+})-induced gelation of two components and the generated IPN skeleton imparted the composite hydrogels with high tissue adhesion, strong structure stability and inhibited rapid leakage of PR and DNase I-PLGA.

With allowing for the prolonged drug release and reducing the frequency of drug administration [17,18], the controlled and sustained release of PR and DNase I were expected since IPN structure imparted fibrin-alginate with applicable and preferable degradation rate catering to the practical demand, which is the primary merit of hydrogels [19–22]. In detail, this IPN hydrogel underwent in situ gelation and degradation over time after injection, followed by the release of DNase I-PLGA nanoparticles and PR to wreck NETs and antagonize catecholamines associated with surgical resection. Through localized NETs degradation and adrenergic nerve signaling antagonism, surgery-induced pro-inflammation plus pro-angiogenesis landscape of tumors niche were extensively abrogated, with which microvessel density decline, MDSCs depletion and NK infiltration promotion were accompanied and CD8$^+$ T cell exhaustion was attenuated (Fig. 1). Contributed by them, PR@DNase I-PLGA@Gel reshaped milieu significantly, inhibited local relapse, attenuated distant and spreading metastasis, and ignited stronger long-term immunological memory protection for tumor rechallenge. Collectively, two new-found reliable targets mattering recurrence and metastasis of postsurgical cancer niches, i.e., NETs and CANTs, were projected and ascertained, and the engineered IPN-structured hydrogel drug depot could wreck NETs and antagonize CANTs to prevent postoperative tumor relapse and metastases, holding high potential in clinical translation.
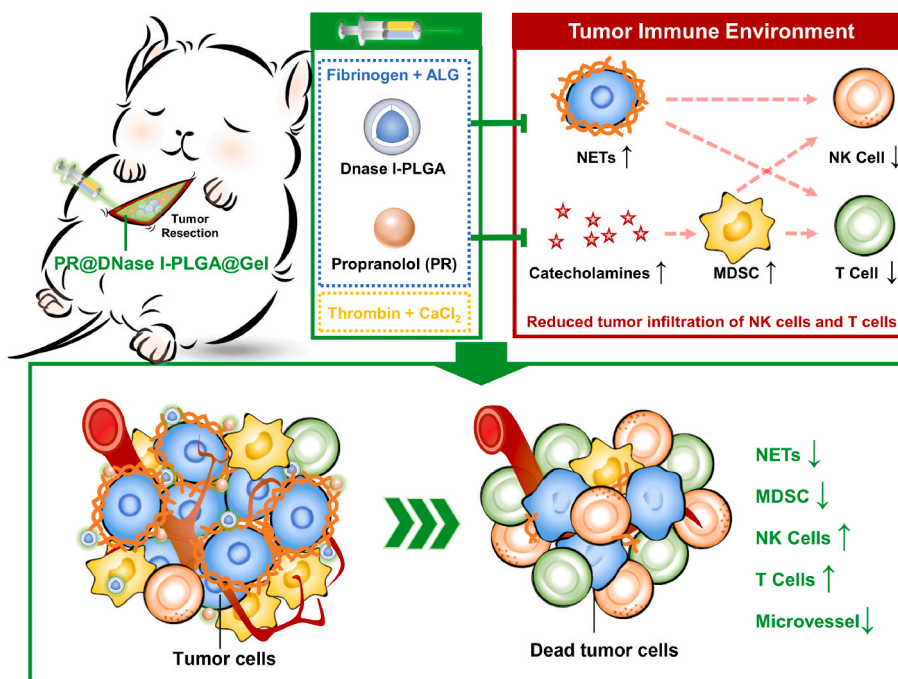

Fig. 1. Schematic of preparing PR@DnaseI-PLGA@Gel for wrecking neutrophil extracellular traps and antagonizing cancer-associated neurotransmitters to prevent postsurgical tumor relapse and metastases. The hydrogel platform can reshape tumor microenvironment by decreasing microvessel density, blocking myeloid-derived suppressor cells, up-regulating the production of various proinflammatory cytokines, enhancing natural killer cell function and relieving cytotoxic T cell exhaustion.

2. Results

2.1. Local tumor progression promotion by SR-induced NET formation and catecholamine release

To uncover the rationale and dominant targets of postsurgical tumor relapse and metastases, we performed an incomplete SR on the pre-clinical model (i.e., 4T1 tumor-bearing model) to simulate the high relapse rate of triple negative breast cancer after surgery in clinical field (Fig. 2a) [23]. Mice in incomplete SR group have greater tumor burden on day 18 compared to the group receiving sham surgery on the contralateral flank of tumor-bearing side. In contrast, there is no obvious tumor volume difference between the sham operation and untreated groups (Fig. 2b–d). Afterwards, we carried out RNA sequencing for determining specific gene pathways involved in local progression of incomplete SR group. A number of 683 upregulated genes and 525 downregulated genes are significantly identified (Fig. S1). Gene Ontology (GO) analysis uncovers a significant enrichment of differentially expressed genes in immune-related functions and pathways in the Biological Process (BP) category. These functions encompass vital processes such as the immune system process, immune response, chemotaxis and particular neutrophil chemotaxis (Fig. 2e). These results clearly indicate a robust correlation between SR and neutrophil-related immune functions. Beyond that, the overexpressed genes in Reactome

enrichment analysis involve VEGF ligand−receptor interactions, neutrophil degranulation and GPCR downstream signaling (Fig. 2f).

Notably, there are significant up-regulations of genes associated with the formation of NETs (*Cxcr1, Cxcr2, CXCL2*) [24], angiogenesis (*Ang2, ANGPT2, VEGFA*), and GPCR activity (*Hcar2, Mrgpra2b*) in the residual tumors (Fig. 2g). In contrast, genes related to beta-adrenergic receptors (ADRs) (*Adra1b* and *Adrb2*) are obviously down-regulated in the SR group, which may be attributed to the overstimulation of ADRs caused by higher circulation levels of cancer-associated catecholamines (norepinephrine (NE) and epinephrine (EPI)) (Fig. 2h and i), as explained by Sousa et al [25]. Next, we used flow cytometry (FCM) and immunofluorescence to observe NETs, tumor vascularization and immunosuppressive niche inside the residual tumor after three days post-SR. Since catecholamines released by sympathetic nerves can activate adrenergic receptors present on almost all cell phenotypes including MDSCs and vascular endothelial cells, circulating norepinephrine and epinephrine may have the capacity to increase MDSC function and angiogenesis in TME [26]. FCM analysis reveals a significant increase in the infiltration of MDSCs in SR-treated tumors compared to untreated tumors (Fig. 2j and k). It is no doubt that NETs index (indicated by myeloperoxidase (MPO) staining) and MDSCs index (indicated by GR-1 staining) are notably higher in the postsurgical tumor samples (Fig. 2l-n). Taken together, these data unveil that SR elicits a complex angiogenesis-inflammatory reaction and promotes the
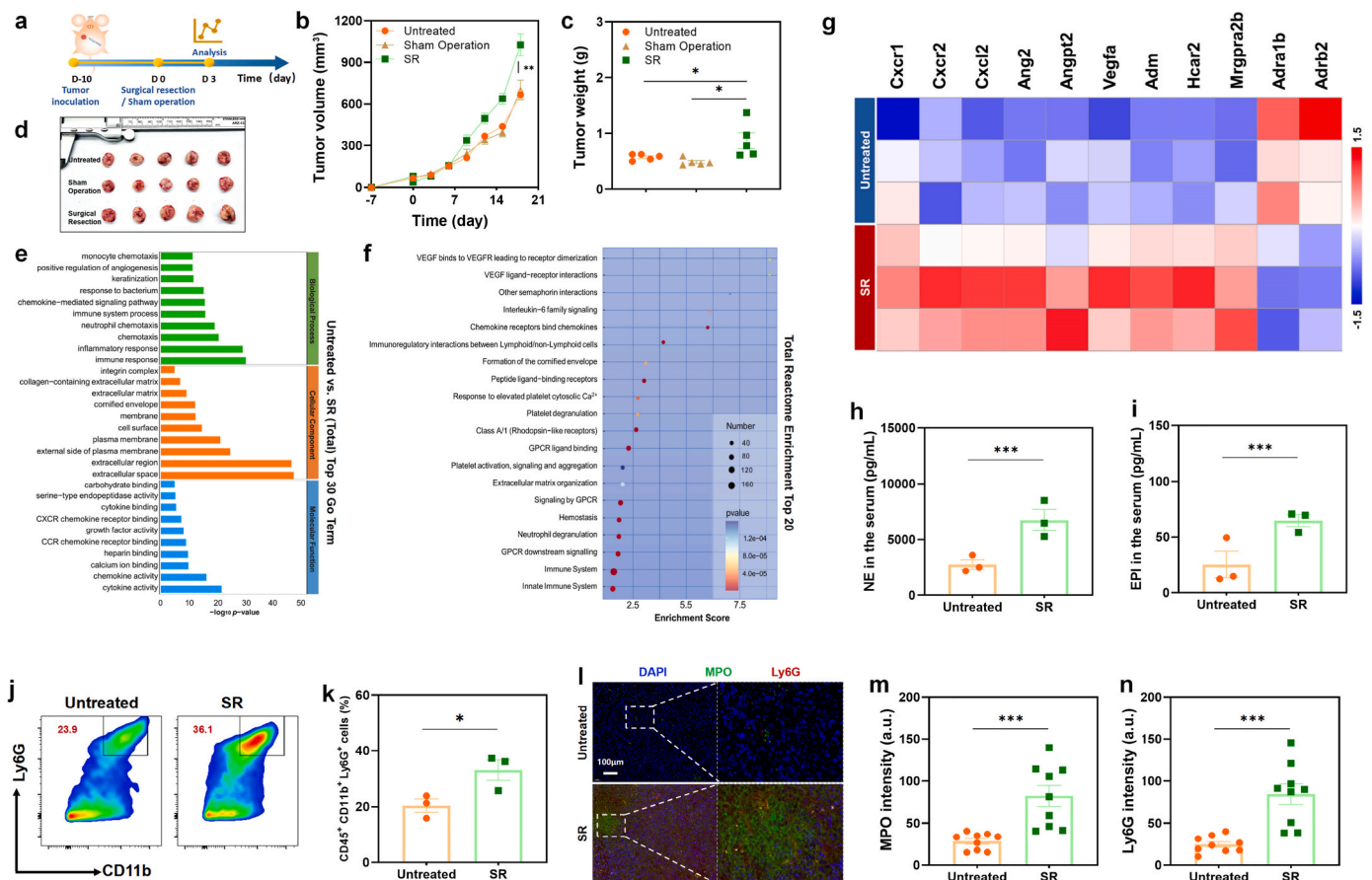

Fig. 2. SR promoting tumor progression and inducing angiogenesis-immunosuppression niche. (a) Schematic illustration of SR treatment; (b) Residual tumor growth kinetics of mice in untreated, sham operation and SR groups (n = 5); (c) Weight of the excised tumor on day 17 after varied treatments (n = 5); (d) Photographs of excised tumors at the end of treatments; (e) Significant enrichment in gene ontology (GO) terms (top 30, n = 3); (f) Reactome analysis for uncovering the affected pathways by above differential genes (top 20, n = 3); (g) Heat map of mean fold-change in gene expression of chemokines and immune suppression (n = 3); (h,i) Quantification of the secretion of NE (h) and EPI (i) in serum from mice in different groups as indicated (n = 3); (j,k) Representative flow cytometric analysis (j) and quantification (k) of MDSCs (CD45⁺CD11b⁺Ly6G⁺) (n = 3); (l) Representative images of MPO (green) and Ly6G (red) immunofluorescence staining and DAPI (blue) nuclear staining after various treatments as indicated; (m,n) Quantification of MPO (m) and Ly6G (n) positive staining signals from the images shown in l (n = 9). Data are expressed as the mean ± standard deviation (SD). Statistical significances were calculated via two-tailed Student's t-tests, *p < 0.05 and ***p < 0.001.

development of residual tissues, wherein NETs formation and circulated catecholamines release in response to resection stress are identified to be two driving forces.

2.2. Preparation of DNase I-PLGA and PR@DNase I-PLGA@Gel

DNase I-PLGA nanoparticles were synthesized by the double emulsion solvent evaporation method. Scanning electron microscopy (SEM) indicate the homogeneous distribution and spherical morphology of nanoparticles (Fig. S2a) with an average size of 266 nm and negatively-charged surface (Figs. S2b and c). Then we investigated the loading capacity and release rate of DNase I in nanoparticles. The entrapment efficiency of DNase I is 74.72 ± 0.98 % and its accumulative release level reaches 72.63 ± 1.54 % within 14 days at room temperature with gentle shaking in neutral PBS (Fig. S3). The DNA degradation capability of DNase I released from DNase I-PLGA nanoparticles was evaluated using agarose gel electrophoresis (Fig. S4). DNase I released from DNase I-PLGA nanoparticles perform like free DNase I to degrade DNA, suggesting that PLGA shell fails to impair the activity of encapsulated DNase I.

IPN-structured fibrin/alginate hydrogel as the drug depot were investigated, and the 10:1 ratio of fibrin/alginate is preferable because of the homogenous IPN without phase splitting (Fig. S5) and desirable degradation is obtained. The composite hydrogel with or without PR and DNase I-loaded PLGA nanoparticles experience instant gelation through a double tube syringe (Fig. 3a and b), wherein thrombin solution (500 U•mL^{-1}) and Ca^{2+} are used the gelation triggers of fibrin and alginate, respectively. The porous network microstructure is observed (Fig. 3c and d), wherein PR and DNase I-loaded PLGA nanoparticles bring about the pore enlargement of IPN structure. A shear rate sweep demonstrates that the viscosity of both hydrogels (blank Gel and PR@DNase I-PLGA@Gel) decreases by over two orders of magnitude in response to increased shear rates, confirming their potential for injectability (Fig. 3e).

Despite pore enlargement, the toughness of fibrin-alginate IPN hydrogels after loading PR and DNase I-loaded PLGA nanoparticles (PR@DNase I-PLGA@Gel) have no obvious difference comparing to blank Gel in the compressive stress-strain test (Fig. 3f). Notably, IPN-
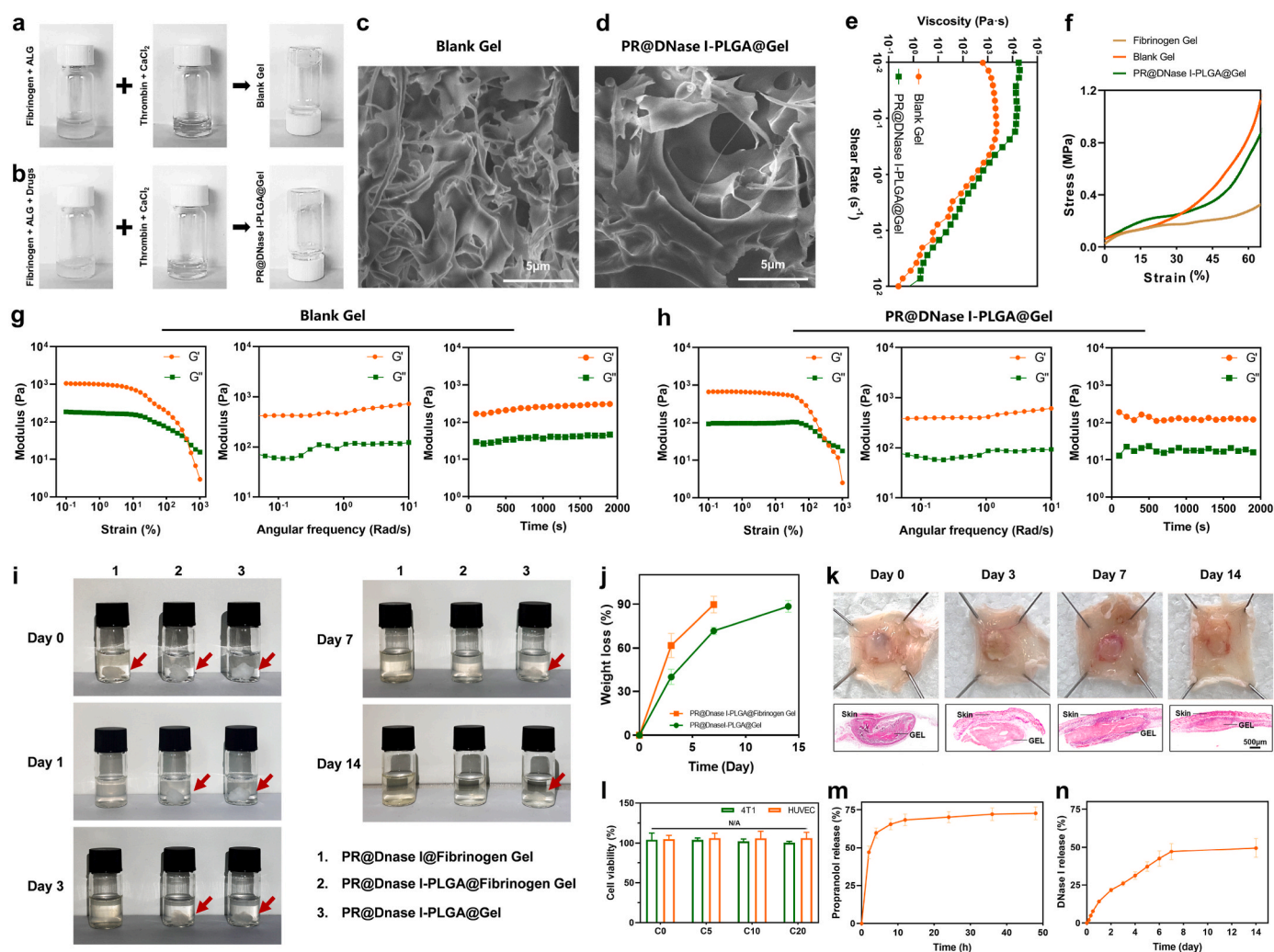

Fig. 3. Synthesis and characterization of in situ formed bioresponsive scaffold. (a,b) Photographs of hydrogel formation without (a) or with (b) drugs; (c,d) Representative SEM image of hydrogels including blank gel (c) and PR@DNaseI-PLGA@Gel (d). (e) Steady shear rheology of different hydrogels; and (f) Compressive stress-strain curves of different hydrogels. (g,h) Rheological behaviors of blank gel (g) and PR@DNaseI-PLGA@Gel (h) as the functions of strain, angular frequency and time. (i) *In vitro* degradation photos of PR@DNase I@Fibrinogen Gel, PR@DNase I-PLGA@Fibrinogen Gel and PR@DNase I-PLGA@Gel in PBS solution over 14 days; and (j) Time-dependent weight loss of PR@DNase I-PLGA@Fibrinogen Gel and PR@DNase I-PLGA@Gel in PBS solution. (k) *In vivo* degradation behavior and tissue biocompatibility of in situ formed PR@DNaseI-PLGA@Gel hydrogel with H&E staining of the surrounding skin at different testing time; (l) The cytotoxicity of lyophilized PR@DNaseI-PLGA@Gel with different dilution; (m,n) Accumulative release of PR (m) and DNase I (n) from PR@DNaseI-PLGA@Gel in PBS solution. Data are presented as means ± SD (n = 3). N/A means no significance.

structured fibrin/alginate hydrogels outperform fibrin hydrogel in compressibility or deformability. Beyond compressibility test, the mechanical strength was monitored and assessed. Strain-dependent, angular frequency-dependent and time-dependent rheology sweep tests reveal that the IPN-structured fibrin-alginate hydrogel with or without PLGA-based nanoparticles share identical mechanical characteristics due to the approximately identical storage (G′) moduli (Fig. 3g and h). Both hydrogels can withstand high deformation since storage (G′) moduli is still larger than loss (G″) moduli under high strain and angular frequency.

The in vitro degradation behaviors of various hydrogels were evaluated in PBS. Without PLGA protection and delayed release, direct entrapment of DNase I rapidly and completely degrades fibrin hydrogel

within 1 days, as evidenced by the comparison between PR@DNase I@Fibrinogen Gel and PR@DNase I-PLGA@Fibrinogen Gel. In contrast, the IPN structure in such composite fibrin/alginate hydrogels (PR@DNase I-PLGA@Gel) shows a delayed degradation due to the enhanced mechanical strength compared to fibrin hydrogels (PR@DNase I-PLGA@Fibrinogen Gel) (Fig. 3i and j). The integrity of IPN-structured fibrin/alginate is kept over 14 days, enabling the continuous drug release, which is desirable for benefiting anti-tumor therapy. Their biocompatibility and biodegradability were further examined in healthy Balb/c mice. The overall size of gel decreases gradually at the injection site over time during 14 days post-injection, suggesting the degradation of fibrin, as indicated in the HE-stained and safranin O-fast green-stained photos (Fig. 3k and S6). Intriguingly,
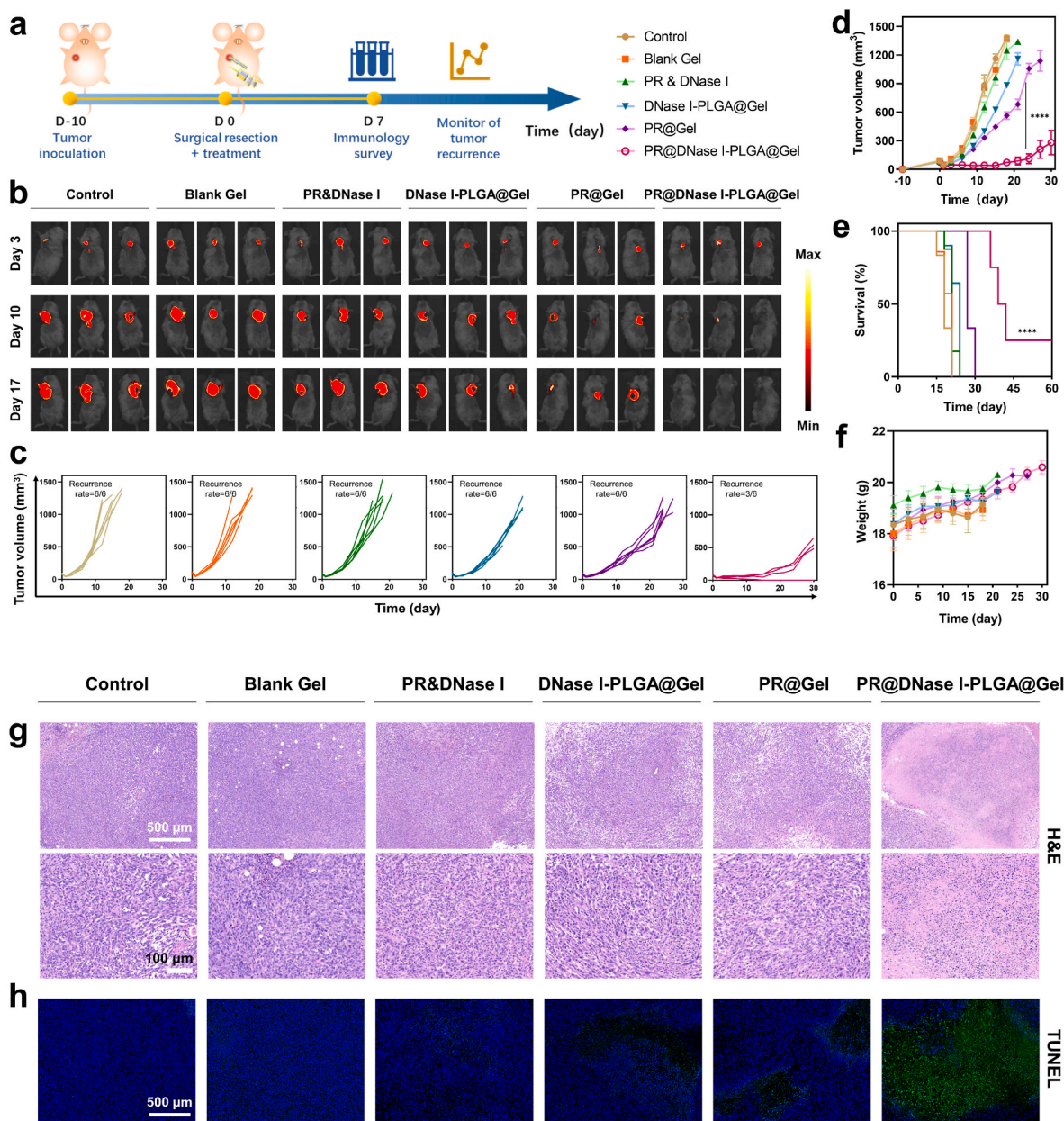

Fig. 4. PR@DNaseI-PLGA@Gel treatment against postsurgical tumor recurrence. (a) Schematic illustration of the experiment design to assess the in vivo PR@DNaseI-PLGA@Gel treatment and its triggered immune responses (PR, 25 mg•kg^{-1}; DNase I, 200 U per mouse); (b) Representative bioluminescence images of fLuc-4T1 tumor after varied treatments as indicated; (c–f) Individual tumor growth kinetics (c), average tumor growth curves (d), Kaplan-Meier survival curves (e) and body weight fluctuation curves (f) of 4T1 tumor-bearing mice after varied treatment strategies (n = 6); (g) Representative H&E histopathological images of 4T1 tumors harvested from mice in different groups: 10x (top) and 30x (bottom) fold magnifications; (h) Representative TUNEL (green) immunofluorescence images of the of 4T1 tumors from mice in different groups. Data are expressed as the mean ± SD. Statistical difference was calculated using two-tailed unpaired student's t-test (d) and Log-rank (Mantel-Cox) test (e), ****$p < 0.0001$.

there are no obvious inflammatory responses since identical infiltration or secretion level of TNFα, IL-6 and mast cell are observed (Fig. 3k and S7). This degradation result re-ascertains the high applicability of IPN degradation rate and the feasibility of continuous drug release. The fibrin-alginate IPN hydrogel alone show no obvious toxicity even at a high dose (Fig. 3l), ensuring the clinical translation potential. Next, we verified the ability of continuous cargo release from the hydrogel, and the gel shows a gradual release of payloads in neutral PBS. Even though 75 % PR is released within 4 days, there is still 25 % PR in hydrogel for continuous release (Fig. 3m), whereas the encapsulations in PLGA and hydrogel allow a sustained release of DNase I that match the hydrogel degradation rate in 14 days (Fig. 3n). The sustained DNase I release is also confirmed in vivo. Compared with the free Cy5-labeled DNase I, the Cy5-labeled DNase I in DNase I-PLGA@Gel can persist in the surgical cavity at least 14 days as shown by fluorescence imaging (Fig. S8). The sequential and sustained release of PR and DNase I might enables synergistic antitumor efficacy under only one administering [27,28].

2.3. PR@DNase I-PLGA@Gel for inhibiting postsurgical tumor relapse

To validate whether the combination of PR and DNase I could prevent breast cancer relapse after incomplete SR, in vivo recurrence inhibition after incomplete SR was surveyed, and procedure is shown in Fig. 4a, wherein only single injection at surgical cavity is carried out. The blank Gel, DNase I-PLGA@Gel, PR@Gel and PR@DNase I-PLGA@Gel were formed in the residual cavity after tumor resection. Tumor growth of mice was firstly monitored by captured

bioluminescence signals from fLuc-4T1 tumors (Fig. 4b). The recurrence tumor of untreated and blank gel-treated mice grows progressively and all die within 3 weeks after incomplete resection of primary tumor. Systematic injection of PR & DNase I has only a slight delay in the recurrence tumor growth. Although DNase I-PLGA@Gel -treated and PR@Gel -treated mice have a modest delay of tumor growth, all mice die within 30 days after the incomplete resection of primary tumor (Fig. 4c–e). In PR@DNase I-PLGA@Gel group, significant tumor recession is achieved and half of mice cured with no detectable tumors (Fig. 4c and d). In addition, no significantly unnatural weight changes were observed in mice after different treatments (Fig. 4f). Significant pathological damages in tumor are also observed in H&E staining (Fig. 4g) and TUNEL staining (Fig. 4h) in PR@DNase I-PLGA@Gel treatment group. To verify in vivo biosafety, the histology analyses are performed on the major organs, and the serum biochemistry assays are executed. There are no appreciable damages observed in the hearts, spleens, kidneys and livers (Fig. S9), and no significant difference is found in serum parameters (Fig. S10), revealing no obvious side effect induced by PR@DNase I-PLGA@Gel treatment.

To delineate the molecular mechanisms of PR@Dnase I-PLGA@Gel in modulating signaling pathways within SR tumor tissues, RNA-seq analyses were conducted, and volcano plot preliminarily uncovers that there are abundant significantly-different genes (Fig. 5a). The subsequent KEGG pathway categorization analysis unveils that the predominant enrichment of differentially expressed genes is located within the immune system (Fig. 5b). Furthermore, Gene Set Enrichment Analysis (GSEA) reveals remarkable downregulations of NETs formation-
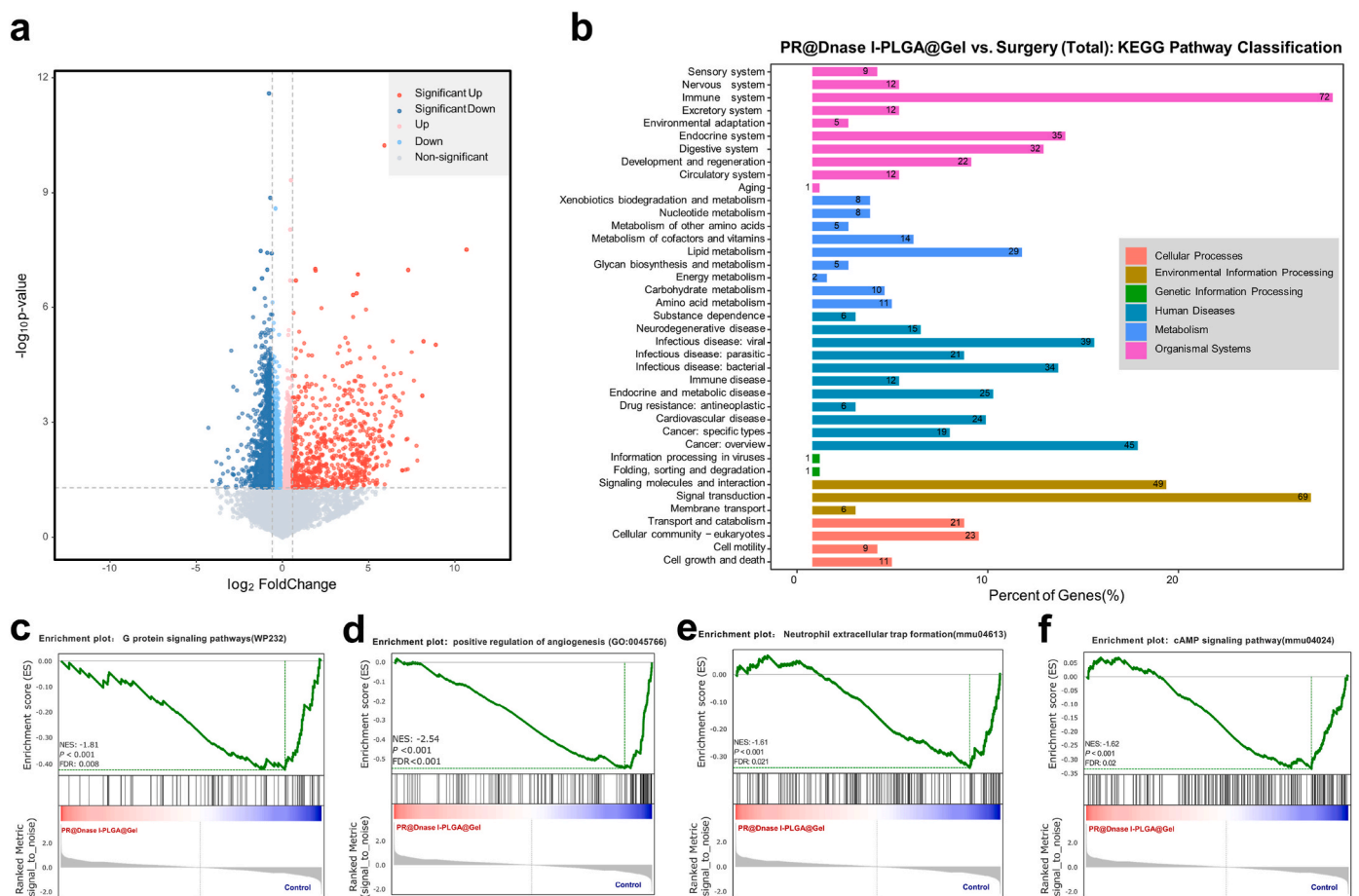

Fig. 5. Sequencing analysis of tumor tissues after PR@Dnase I-PLGA@Gel treatment and Gene Set Enrichment Analysis (GSEA) validations. (a) Volcano plot of treated samples after mRNA sequencing of indicated groups (n = 5); (b) KEGG pathway classification analysis of treated samples after mRNA sequencing of indicated groups; (c) Enrichment results for G protein signaling pathways via GSEA; (d) Enrichment results for positive regulation of angiogenesis via GSEA; (e) Enrichment results for neutrophil extracellular trap formation via GSEA; (f) Enrichment results for cAMP signaling pathway via GSEA.

associated pathways including cAMP, G protein, as well as the positive regulation of angiogenesis in the PR@Dnase I-PLGA@Gel-treated group, as opposed to the SR group (Fig. 5c–f).

2.4. PR@DNase I-PLGA@Gel for inducing postsurgical anti-tumor immune responses

To further reveal the underlying mechanisms of anticancer responses induced by this localized PR@DNase I-PLGA@Gel treatment, residual tumors were harvested on day 7 post-treatment. Immunofluorescence staining analysis for MPO, CD34 and tyrosine hydroxylase antibody

(TH) that are the markers of NETs, vascular endothelium and adrenergic nerves were firstly performed, respectively (Fig. 6a–c). It is found that PR@DNase I-PLGA@Gel group significantly downregulates MPO expression ($p < 0.0001$) in residual 4T1 tumor when compared with the PR@Gel group, illustrating that the sustained release of DNase I effectively causes NETs destruction (Fig. 6a–d). PR@DNase I-PLGA@Gel and PR@Gel treatments significantly decrease CD34 expression when compared to the controls (Fig. 6b–e). The fluorescence intensity of TH expression was also significantly decreased in the PR loaded gel groups (PR@DNase I-PLGA@Gel and PR@Gel) compared with other groups (Fig. 6c–f). All these results adequately uncover that PR@DNase I-
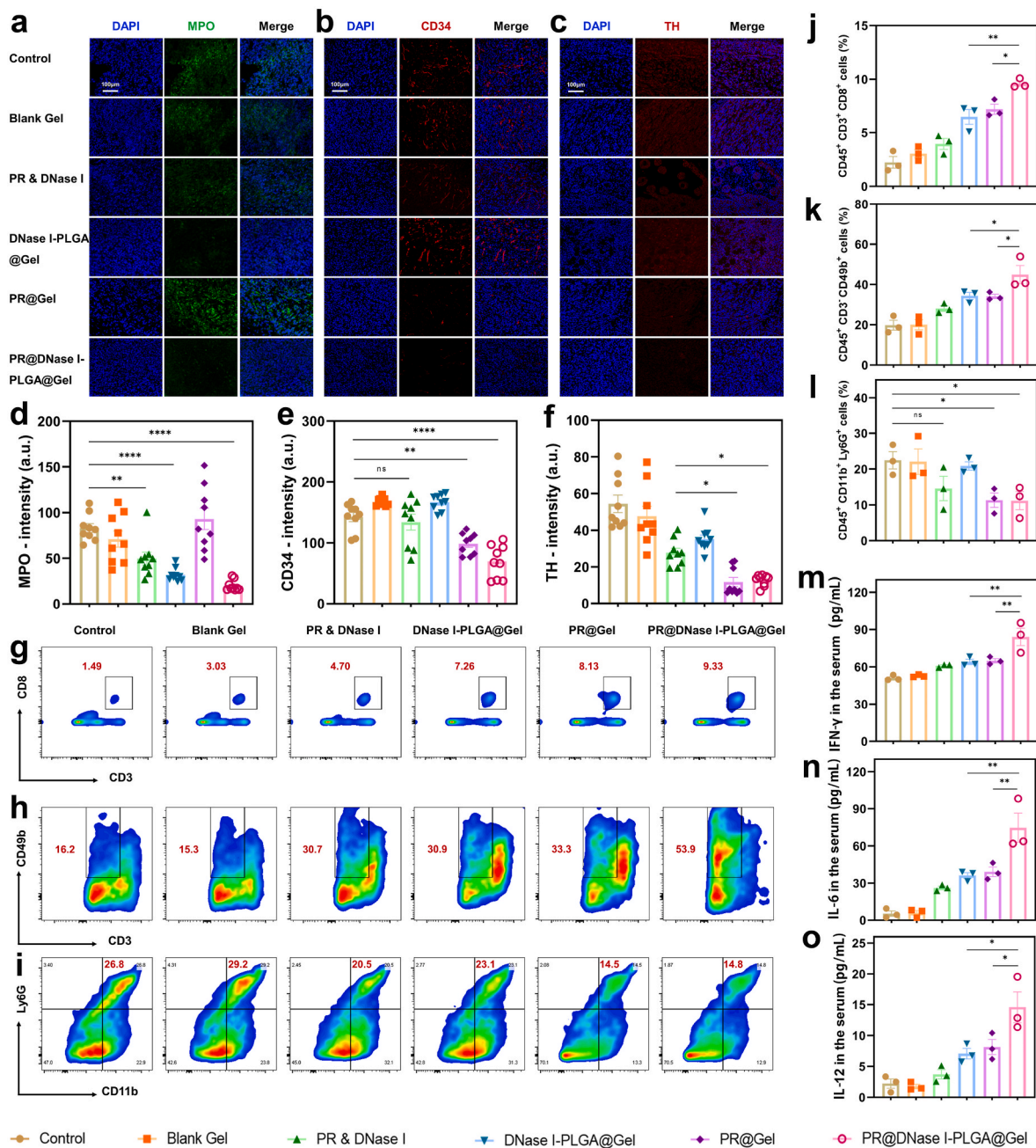

Fig. 6. The robust antitumor immune responses triggered by PR@DNaseI-PLGA@Gel treatment. (a–c) Representative images of MPO (green) (a), CD34 (red) (b) and TH (red) (c) immunofluorescence straining and DAPI (blue) nuclear staining after various treatments as indicated; (d–f) Quantification of MPO (d), CD34 (e), TH (f) positive staining signals from the images shown in a-c (n = 9); (g–i) Representative flow cytometric analysis of CD8$^+$ T cells (CD45$^+$CD3$^+$CD8$^+$) (g), NK cells (CD45$^+$CD3$^-$CD49b$^+$) (h) and MDSCs (CD45$^+$CD11b$^+$Ly6G$^+$) (i); (j–l) Corresponding flow cytometric quantification of CD8$^+$ T cells (j), NK cells (k) and MDSCs (l) (n = 3). (m–o) Cytokine levels of secreted IFN-γ (m), IL-6 (n), IL-12 (o) in serum from mice after various treatments as indicated in the figure (n = 3). Data are expressed as the mean ± SD. Statistical significances were calculated via two-tailed Student's t-tests and One-way ANOVA, *$p < 0.05$, **$p < 0.01$ and ****$p < 0.0001$.

PLGA@Gel is conferred with abilities to wreck NETs, decrease microvessel density and antagonize adrenergic nerves.

Tumor immune environment were tracked by FCM after different kinds of treatments. PR@DNase I-PLGA@Gel effectively enhance the infiltrations of tumor-infiltrating CD8$^+$ T cells (CD45$^+$CD3$^+$CD8$^+$) (p < 0.0001), NK cells (CD45$^+$CD3$^-$CD49b$^+$) (p < 0.0001), and coincidently oppose the infiltration of MDSCs (CD45$^+$CD11b$^+$Ly6G$^+$) (p = 0.0407) (Fig. 6g–l). This inspiring phenomenon suggests our PR@DNase I-PLGA@Gel treatment can significantly improve anticancer immune homeostasis and efficiently hinder MDSC recruitment. Identical results are further obtained by immunofluorescence analysis (Figs. S11 and S12). Furthermore, increased interferon-gamma (IFN-γ), interleukin-6 (IL-6) and interleukin-12 (IL-12) levels in serum of mice treated with PR@DNase I-PLGA@Gel are found (Fig. 6m–o), which once again verify that the robust immune responses activation triggered by the localized treatment strategy is responsible for the excellent recurrence inhibition and survival prolongation.

2.5. PR@DNase I-PLGA@Gel for inducing durable immune-memory effect against postoperative metastasis on abscopal and lung metastasis models

To inspect the immune memory response caused by PR@DNase I-PLGA@Gel therapy, we re-challenged the cured mice after PR@DNase I-PLGA@Gel treatment on day 60, with naive mice injected equal number of 4T1 cells as control (Fig. S13a). As expected, the tumor growth of cured mice exhibits a considerably-elevated inhibition compared with naive mice, and one out of three mice after PR@DNase I-PLGA@Gel therapy is completely resistant to the rechallenge (Figs. S13b–c). The spleen tissues of mice were collected at the end point to understand the underlying long-term memory immunological mechanism after analysis by FCM. The increase of effector memory T cells (CD8$^+$CD62L$^-$CD44$^+$) is observed in cured mice (Fig. S14), which can rapidly respond and provide immediate protections against the secondary invasive cancer cells. This in situ PR@DNase I-PLGA@Gel not only causes local tumor regression, but also prevents tumor rechallenge.

We further explored whether this local treatment could inhibit distant tumor progression by activating systemic anticancer immunity. Herein, a bilateral fLuc-4T1 tumor-bearing mice model was established. Three days after the primary tumor inoculation (on the right flank), a second tumor was implanted on the left flank to mimic the distant tumor (Fig. 7a). The right primary tumors were treated as before, where the fLuc-4T1 tumor-bearing mice randomly were divided into four groups: Control, DNase I-PLGA@Gel, PR@Gel and PR@DNase I-PLGA@Gel. Although DNase I-PLGA@Gel and PR@Gel therapy could suppress the primary tumor to some extent, they fail to significantly inhibit the growth of distant tumors. On the contrary, the PR@DNase I-PLGA@Gel therapy not only prominently inhibits the progression of primary tumors, but also remarkably slows down the outgrowth of distant tumors (Fig. 7b–d) with the lowest tumor weight and volume (Fig. 7b–d and S15). The variation trend of tumor volume keeps pace with that of tumor weight (Fig. S15). To elucidate the abscopal inhibition mechanism of PR@DNase I-PLGA@Gel, immune cells in distant tumors were evaluated one week after treating the primary tumor. FCM data display a remarkable increase in the number of infiltrated CD8$^+$ T cells (CD45$^+$CD3$^+$CD8$^+$) in the PR@DNase I-PLGA@Gel group compared with DNase I-PLGA@Gel group (p = 0.004) and PR@Gel group (p = 0.004) (Fig. 7e and f). Beyond that, the population of NK cells (CD45$^+$CD3$^-$CD49b$^+$) in PR@DNase I-PLGA@Gel group is also remarkably increased (Fig. 7g,h), and a substantial decrease of MDSCs (CD45$^+$CD11b$^+$Ly6G$^{+)}$ in distant tumors after PR@DNase I-PLGA@Gel treatment is obtained (Fig. 7i and j) when comparing to other groups.

Encouraged by the excellent immune activation and immune memory effects of PR@DNase I-PLGA@Gel in inhibiting the progression of primary and distant tumors, we further investigated the efficacy of preventing lung metastases. The lung tissues of primary and distant tumor-bearing mice were collected at the end point, and bioluminescence images of fLuc-4T1 lung metastasis were captured and the number of nodules were counted (Fig. 7k,l). The fluorescence images and quantitative results directly verify that PR@DNase I-PLGA@Gel treatment receive the least number of nodules (Fig. 7l), thus exerting the most potent immune responses against lung metastasis.

3. Discussion

ECM have been found encompass many targets associated with postsurgical tumor relapse including physical escape targets associated with physical characteristic (viscosity, stiffness, etc.), and chemical escape targets associated with chemical components (e.g., cell adhesion factor, cell adhesion factor, etc.) [29–31], which reprogramme the TME and render it unfavorable for immunotherapy [32–39]. Although several technologies have been developed to address these apparent events associated immunosuppressive TME, the underlying mechanisms or targets remain unclear and unresolved [40,41]. In this report, NETs and CANTs were screened and ascertained as the dominant targets to shape the immunosuppressive TME and reprogramme unfavorable ECM associated with postsurgical tumor relapse and metastases. More significantly, targetedly degrading NETs and blocking CANTs were enabled by this in-situ IPN-structured fibrin/alginate hydrogel drug depot loading PR and DNase I-loaded PLGA nanoparticles.

As an integral component of the host defense system, DNase I plays a crucial role in digesting the DNA backbone of NETs. This highlights its potential as a therapeutic intervention for diseases associated with NETs, such as sepsis or thrombosis [42,43]. However, the low serum stability of DNase I hinders its large-scale clinical applications. On the other hand, as a non-specific β1-and β2-ADR antagonist [44], although PR could serve as an adjuvant in cancer management [45], systematic administration of PR resultied in more side-effects and lethal outcomes [46]. Herein, we proposed this localized hydrogel delivery system with matched degradation rate, which not only concentrated DNase I and PR, but also released DNase I and PR in a sustained manner to repress residual tumors after SR.

4. Conclusions

In summary, our findings strongly agree with the fact that elevated NETs formation and CANTs (catecholamines) are predominantly responsible for angiogenesis-immunosuppressive residual niche development, leading to more aggressive SR-related tumor relapse and metastases by utilizing preclinical models. This study provided proof of concept that combinational delivery of NETs inhibitor (DNase I) and catecholamines antagonist (PR) could serve as an efficient approach to address this issue. Thus, IPN-structured fibrin/alginate hydrogel drug depot (PR@DNase I-PLGA@Gel) was successfully constructed to achieve a specific and sustained release of DNase I and PR in the residual disease after SR for wrecking NETs and antagonizing CANTs. The proposed PR@DNase I-PLGA@Gel significantly suppressed locally residual and distant tumors, induced strong immune memory effects and inhibited lung metastasis. To explore underlying mechanisms, PR@DNase I-PLGA@Gel was capable of decreasing microvessel density, blocking myeloid-derived suppressor cells, up-regulating the production of various proinflammatory cytokines, enhancing NK cell function and relieving cytotoxic T cell exhaustion. Therefore, considering the fact that SR is the primary option for most early-stage solid tumors, this IPN-based hydrogel drug depot provides a reasonable rationale to unlock targeted NETs degradation and catecholamines blocking, and pave a solid foundation to overcome incomplete resection-mediated angiogenetic and immunosuppressive TME, improving the effectiveness of preventing postsurgical tumor relapse and metastases.
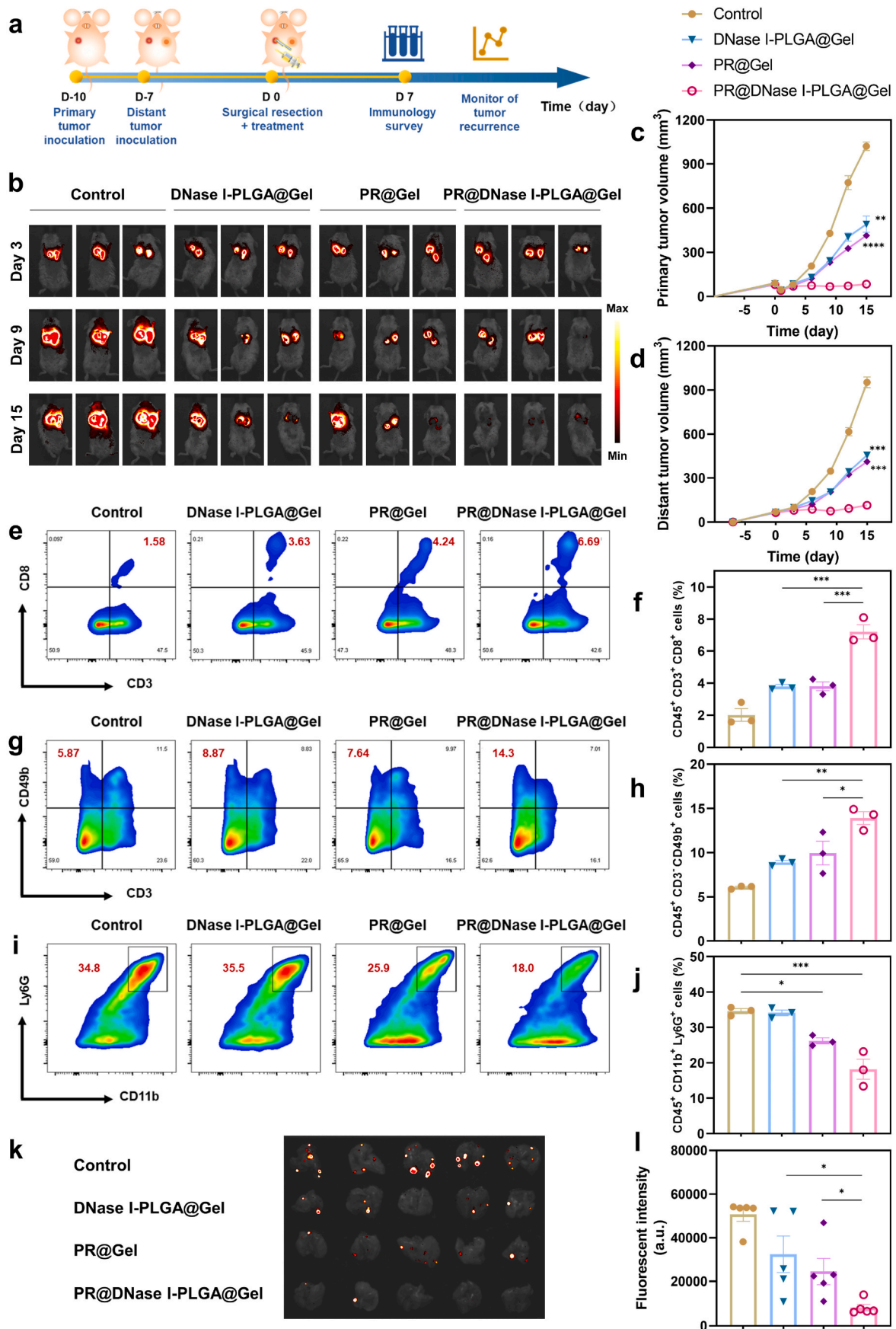
(caption on next page)

Fig. 7. PR@DNaseI-PLGA@Gel stimulating the systemic immune memory effects to oppose tumor challenge and lung metastasis. (a) Schematic illustration of PR@DNaseI-PLGA@Gel therapy to inhibit distant tumor growth in a mouse model of SR; (b) Representative bioluminescence images of fLuc-4T1 tumor bearing mice from each group after varied treatments every 6 days from days 3–15; (c,d) Average tumor growth curves of primary (c) and distant (d) tumors (n = 5); (e) Representative flow cytometric analysis and (f) quantification of $CD8^+$ T cells ($CD45^+CD3^+CD8^+$); (g) Representative flow cytometric analysis and (h) quantification of NK cells ($CD45^+CD3^-CD49b^+$); (i) Representative flow cytometric analysis and (j) quantification of MDSCs ($CD45^+CD11b^+Ly6G^+$). (k) Fluorescence images of metastatic lungs *ex vivo*; (l) The relative luciferase intensity in the excised lung tissues from different groups (n = 5). Data are expressed as the mean ± SD. Statistical significances were calculated via two-tailed Student's t-tests and One-way ANOVA, $*p < 0.05$, $**p < 0.01$, $***p < 0.001$ and $****p < 0.0001$.

Experimental section

All materials, experimental methods are included in supporting information.

Financial support

Ethics approval and consent to participate

All animal experiments were approved by the Laboratory Animal Center in Tenth People's Hospital affiliated from Tongji University School of Medicine with an approval number: SHDSYY-2023-3429-KR0246.

Data availability statement

The data are available from the corresponding author upon reasonable request.

CRediT authorship contribution statement

Hang Zhou: Writing – original draft, Validation, Software, Resources, Methodology, Investigation, Formal analysis, Data curation. **Chunyan Zhu:** Investigation, Formal analysis, Data curation. **Qing Zhao:** Resources, Methodology, Investigation, Data curation, Conceptualization. **Jinliang Ni:** Investigation, Data curation. **Haipeng Zhang:** Formal analysis, Data curation. **Guangcan Yang:** Project administration, Methodology, Formal analysis. **Jianchao Ge:** Validation, Resources, Investigation. **Chao Fang:** Project administration, Investigation, Data curation. **Hong Wei:** Visualization, Resources. **Xianli Zhou:** Funding acquisition. **Kun Zhang:** Writing – review & editing, Validation, Supervision, Project administration, Funding acquisition, Formal analysis, Conceptualization.

Declaration of competing interest

The authors declare no conflict of interest.

Appendix A. Supplementary data

Supplementary data to this article can be found online at https://doi.org/10.1016/j.bioactmat.2024.05.022.

References

[1] S. Loibl, P. Poortmans, M. Morrow, C. Denkert, G. Curigliano, Breast cancer, Lancet 397 (2021) 1750–1769, https://doi.org/10.1016/s0140-6736(20)32381-3.

[2] M. Mannino, J. Yarnold, Effect of breast-duct anatomy and wound-healing responses on local tumour recurrence after primary surgery for early breast cancer, Lancet Oncol. 10 (2009) 425–429, https://doi.org/10.1016/s1470-2045(09)70040-3.

[3] J.G. Hiller, N.J. Perry, G. Poulogiannis, B. Riedel, E.K. Sloan, Perioperative events influence cancer recurrence risk after surgery, Nat. Rev. Clin. Oncol. 15 (2018) 205–218, https://doi.org/10.1038/nrclinonc.2017.194.

[4] T.E. Sutherland, D.P. Dyer, J.E. Allen, The extracellular matrix and the immune system: a mutually dependent relationship, Science 379 (2023) eabp8964, https://doi.org/10.1126/science.abp8964.

[5] F. Tang, Y. Tie, W.Q. Hong, Y.Q. Wei, C.Q. Tu, X.W. Wei, Targeting myeloid-derived suppressor cells for premetastatic niche disruption after tumor resection, Ann. Surg Oncol. 28 (2021) 4030–4048, https://doi.org/10.1245/s10434-020-09371-z.

[6] H. Voss, M. Wurlitzer, D.J. Smit, F. Ewald, M. Alawi, M. Spohn, D. Indenbirken, M. Omidi, K. David, H. Juhl, R. Simon, G. Sauter, L. Fischer, J.R. Izbicki, M. P. Molloy, B. Nashan, H. Schluter, M. Jucker, Differential regulation of extracellular matrix proteins in three recurrent liver metastases of a single patient with colorectal cancer, Clin. Exp. Metastasis 37 (2020) 649–656, https://doi.org/10.1007/s10585-020-10058-8.

[7] V. Papayannopoulos, Neutrophil extracellular traps in immunity and disease, Nat. Rev. Immunol. 18 (2018) 134–147, https://doi.org/10.1038/nri.2017.105.

[8] Y. Cheng, Y. Gong, X. Chen, Q. Zhang, X. Zhang, Y. He, L. Pan, B. Ni, F. Yang, Y. Xu, L. Zhou, Y. Yang, W. Chen, Injectable adhesive hemostatic gel with tumor acidity neutralizer and neutrophil extracellular traps lyase for enhancing adoptive NK cell therapy prevents post-resection recurrence of hepatocellular carcinoma, Biomaterials 284 (2022) 121506, https://doi.org/10.1016/j.biomaterials.2022.121506.

[9] C. Kaltenmeier, H.O. Yazdani, K. Morder, D.A. Geller, R.L. Simmons, S. Tohme, Neutrophil extracellular traps promote T cell exhaustion in the tumor microenvironment, Front. Immunol. 12 (2021) 785222, https://doi.org/10.3389/fimmu.2021.785222.

[10] J. Albrengues, M.A. Shields, D. Ng, C.G. Park, A. Ambrico, M.E. Poindexter, P. Upadhyay, D.L. Uyeminami, A. Pommier, V. Küttner, E. Bružas, L. Maiorino, C. Bautista, E.M. Carmona, P.A. Gimotty, D.T. Fearon, K. Chang, S.K. Lyons, K. E. Pinkerton, L.C. Trotman, M.S. Goldberg, J.T. Yeh, M. Egeblad, Neutrophil extracellular traps produced during inflammation awaken dormant cancer cells in mice, Science 361 (2018) eaao4227, https://doi.org/10.1126/science.aao4227.

[11] Á. Teijeira, S. Garasa, M. Gato, C. Alfaro, I. Migueliz, A. Cirella, C. de Andrea, M. C. Ochoa, I. Otano, I. Etxeberria, M.P. Andueza, C.P. Nieto, L. Resano, A. Azpilikueta, M. Allegretti, M. de Pizzol, M. Ponz-Sarvisé, A. Rouzaut, M. F. Sanmamed, K. Schalper, M. Carleton, M. Mellado, M.E. Rodriguez-Ruiz, P. Berraondo, J.L. Perez-Gracia, I. Melero, CXCR1 and CXCR2 chemokine receptor agonists produced by tumors induce neutrophil extracellular traps that interfere with immune cytotoxicity, Immunity 52 (2020) 856–871.e858, https://doi.org/10.1016/j.immuni.2020.03.001.

[12] M. Horowitz, E. Neeman, E. Sharon, S. Ben-Eliyahu, Exploiting the critical perioperative period to improve long-term cancer outcomes, Nat. Rev. Clin. Oncol. 12 (2015) 213–226, https://doi.org/10.1038/nrclinonc.2014.224.

[13] H. Mohammadpour, C.R. MacDonald, G. Qiao, M. Chen, B. Dong, B.L. Hylander, P. L. McCarthy, S.I. Abrams, E.A. Repasky, β2 adrenergic receptor-mediated signaling regulates the immunosuppressive potential of myeloid-derived suppressor cells, J. Clin. Invest. 129 (2019) 5537–5552, https://doi.org/10.1172/jci129502.

[14] Y. Xia, Y. Wei, Z.Y. Li, X.Y. Cai, L.L. Zhang, X.R. Dong, S. Zhang, R.G. Zhang, R. Meng, F. Zhu, G. Wu, Catecholamines contribute to the neovascularization of lung cancer via tumor-associated macrophages, Brain Behav. Immun. 81 (2019) 111–121, https://doi.org/10.1016/j.bbi.2019.06.004.

[15] D. Marvel, D.I. Gabrilovich, Myeloid-derived suppressor cells in the tumor microenvironment: expect the unexpected, J. Clin. Invest. 125 (2015) 3356–3364, https://doi.org/10.1172/jci80005.

[16] P.H. Thaker, L.Y. Han, A.A. Kamat, J.M. Arevalo, R. Takahashi, C. Lu, N. B. Jennings, G. Armaiz-Pena, J.A. Bankson, M. Ravoori, W.M. Merritt, Y.G. Lin, L. S. Mangala, T.J. Kim, R.L. Coleman, C.N. Landen, Y. Li, E. Felix, A.M. Sanguino, R. A. Newman, M. Lloyd, D.M. Gershenson, V. Kundra, G. Lopez-Berestein, S. K. Lutgendorf, S.W. Cole, A.K. Sood, Chronic stress promotes tumor growth and angiogenesis in a mouse model of ovarian carcinoma, Nat. Med. 12 (2006) 939–944, https://doi.org/10.1038/nm1447.

[17] A.P. Dhand, J.H. Galarraga, J.A. Burdick, Enhancing biopolymer hydrogel functionality through interpenetrating networks, Trends Biotechnol. 39 (2021) 519–538, https://doi.org/10.1016/j.tibtech.2020.08.007.

[18] K. Ma, A.L. Titan, M. Stafford, C. Zheng, M.E. Levenston, Variations in chondrogenesis of human bone marrow-derived mesenchymal stem cells in fibrin/alginate blended hydrogels, Acta Biomater. 8 (2012) 3754–3764, https://doi.org/10.1016/j.actbio.2012.06.028.

[19] H. Cao, L. Duan, Y. Zhang, J. Cao, K. Zhang, Current hydrogel advances in physicochemical and biological response-driven biomedical application diversity, Signal Transduct. Targeted Ther. 6 (2021) 426, https://doi.org/10.1038/s41392-021-00830-x.

[20] M. Yang, Y. Zhang, C. Fang, L. Song, Y. Wang, L. Lu, R.X. Yang, Z.T. Bu, X.Y. Liang, K. Zhang, Q. Fu, Urine-microenvironment-initiated composite hydrogel patch

reconfiguration propels scarless memory repair and reinvigoration of the urethra, Adv. Mater. 34 (2022) 2109522, https://doi.org/10.1002/adma.202109522.

[21] K. Zhang, Y. Fang, Y. He, H. Yin, X. Guan, Y. Pu, B. Zhou, W. Yue, W. Ren, D. Du, H. Li, C. Liu, L. Sun, Y. Chen, H. Xu, Extravascular gelation shrinkage-derived internal stress enables tumor starvation therapy with suppressed metastasis and recurrence, Nat. Commun. 10 (2019) 5380, https://doi.org/10.1038/s41467-019-13115-3.

[22] L. Zheng, S. Liu, X. Cheng, Z. Qin, Z. Lu, K. Zhang, J. Zhao, Intensified stiffness and photodynamic provocation in a collagen-based composite hydrogel drive chondrogenesis, Adv. Sci. 6 (2019) 1900099, https://doi.org/10.1002/advs.201900099.

[23] A.G. Waks, E.P. Winer, Breast cancer treatment: a review, JAMA 321 (2019) 288–300, https://doi.org/10.1001/jama.2018.19323.

[24] Y. Zhang, L. Guo, Q. Dai, B. Shang, T. Xiao, X. Di, K. Zhang, L. Feng, J. Shou, Y. Wang, A signature for pan-cancer prognosis based on neutrophil extracellular traps, J. Immunother. Cancer 10 (2022) e004210, https://doi.org/10.1136/jitc-2021-004210.

[25] D.M. Sousa, V. Fernandes, C. Lourenço, C. Carvalho-Maia, H. Estevão-Pereira, J. Lobo, M. Cantante, M. Couto, F. Conceição, C. Jerónimo, L. Pereira, M. Lamghari, Profiling the adrenergic system in breast cancer and the development of metastasis, Cancers 14 (2022), https://doi.org/10.3390/cancers14225518.

[26] M. Cao, W. Huang, Y. Chen, G. Li, N. Liu, Y. Wu, G. Wang, Q. Li, D. Kong, T. Xue, N. Yang, Y. Liu, Chronic restraint stress promotes the mobilization and recruitment of myeloid-derived suppressor cells through β-adrenergic-activated CXCL5-CXCR2-Erk signaling cascades, Int. J. Cancer 149 (2021) 460–472, https://doi.org/10.1002/ijc.33552.

[27] J. Chen, X. Yu, X.Y. Liu, J.L. Ni, G.C. Yang, K. Zhang, Advances in nanobiotechnology-propelled multidrug resistance circumvention of cancer, Nanoscale 14 (2022) 12984–12998, https://doi.org/10.1039/d2nr04418h.

[28] W.-W. Ren, S.-H. Xu, L.-P. Sun, K. Zhang, Ultrasound-based drug delivery system, Curr. Med. Chem. 29 (2022) 1342–1351, https://doi.org/10.2174/0929867328666210617103905.

[29] D. Wang, M. Zhang, G. Qiu, C. Rong, X. Zhu, G. Qin, C. Kong, J. Zhou, X. Liang, Z. Bu, J. Liu, T. Luo, J. Yang, K. Zhang, Extracellular matrix viscosity reprogramming by in situ Au bioreactor-boosted microwavegenetics disables tumor escape in CAR-T immunotherapy, ACS Nano 17 (2023) 5503–5516, https://doi.org/10.1021/acsnano.2c10845.

[30] M.Y. Wu, H.X. Zhang, C.J. Tie, C.H. Yan, Z.T. Deng, Q. Wan, X. Liu, F. Yan, H. R. Zheng, MR imaging tracking of inflammation-activatable engineered neutrophils for targeted therapy of surgically treated glioma, Nat. Commun. 9 (2018) 4777, https://doi.org/10.1038/s41467-018-07250-6.

[31] J. Xue, Z. Zhao, L. Zhang, L. Xue, S. Shen, Y. Wen, Z. Wei, L. Wang, L. Kong, H. Sun, Q. Ping, R. Mo, C. Zhang, Neutrophil-mediated anticancer drug delivery for suppression of postoperative malignant glioma recurrence, Nat. Nanotechnol. 12 (2017) 692–700, https://doi.org/10.1038/nnano.2017.54.

[32] C. Fang, G. Xiao, T. Wang, L. Song, B. Peng, B. Xu, K. Zhang, Emerging Nano-/bio-Technology Drives Oncolytic Virus-Activated & Combined Cancer Immunotherapy, Research, vol. 6, 2023, p. 108, https://doi.org/10.34133/research.0108.

[33] D. Wang, G. Qiu, X. Zhu, Q. Wang, C. Zhu, C. Fang, J. Liu, K. Zhang, Y. Liu, Macrophage-inherited exosome excise tumor immunosuppression to expedite immune-activated ferroptosis, J. Immunother. Cancer 11 (2023) e006516, https://doi.org/10.1136/jitc-2022-006516.

[34] D. Wang, M. Zhang, Y. Zhang, G. Qiu, J. Chen, X. Zhu, C. Kong, X. Lu, X. Liang, L. Duan, C. Fang, J. Liu, K. Zhang, T. Luo, Intraparticle double-scattering-decoded

[35] X. Yu, C. Fang, K. Zhang, C.X. Su, Recent advances in nanoparticles-based platforms targeting the PD-1/PD-L1 pathway for cancer treatment, Pharmaceutics 14 (2022) 1581, https://doi.org/10.3390/pharmaceutics14081581.

[36] H. Wu, H.Y. Li, Y.Q. Liu, J.C. Liang, Q.S. Liu, Z.G. Xu, Z.Z. Chen, X. Zhang, K. Zhang, C.A. Xu, Blockading a new NSCLC immunosuppressive target by pluripotent autologous tumor vaccines magnifies sequential immunotherapy, Bioact. Mater. 13 (2022) 223–238, https://doi.org/10.1016/j.bioactmat.2021.10.048.

[37] L. Song, L. Lu, Y.Y. Pu, H.H. Yin, K. Zhang, Nanomaterials-based tumor microenvironment modulation for magnifying sonodynamic therapy, Acc. Mater. Res. 3 (2022) 971–985, https://doi.org/10.1021/accountsmr.2c00106.

[38] X. Zhang, Q. Zhao, J. Yang, T. Wang, F. Chen, K. Zhang, Tumor microenvironment-triggered intratumoral in-situ biosynthesis of inorganic nanomaterials for precise tumor diagnostics, Coord. Chem. Rev. 484 (2023) 215115, https://doi.org/10.1016/j.ccr.2023.215115.

[39] Y. Zhang, C. Fang, W. Zhang, K. Zhang, Emerging pyroptosis-engineered nanobiotechnologies regulate cancers and inflammatory diseases: a double-edged sword, Matter 5 (2022) 3740–3774, https://doi.org/10.1016/j.matt.2022.08.026.

[40] Q. Chen, C. Wang, X.D. Zhang, G.J. Chen, Q.Y. Hu, H.J. Li, J.Q. Wang, D. Wen, Y. Q. Zhang, Y.F. Lu, G. Yang, C. Jiang, J. Wang, G. Dotti, Z. Gu, In situ sprayed bioresponsive immunotherapeutic gel for post-surgical cancer treatment, Nat. Nanotechnol. 14 (2019) 89–97, https://doi.org/10.1038/s41565-018-0319-4.

[41] H.T. Ruan, Q.Y. Hu, D. Wen, Q. Chen, G.J. Chen, Y.F. Lu, J.Q. Wang, H. Cheng, W. Y. Lu, Z. Gu, A dual-bioresponsive drug-delivery depot for combination of epigenetic modulation and immune checkpoint blockade, Adv. Mater. 31 (2019) 1806957, https://doi.org/10.1002/adma.201806957.

[42] W. Meng, A. Paunel-Görgülü, S. Flohé, A. Hoffmann, I. Witte, C. MacKenzie, S. E. Baldus, J. Windolf, T.T. Lögters, Depletion of neutrophil extracellular traps in vivo results in hypersusceptibility to polymicrobial sepsis in mice, Crit. Care 16 (2012) R137, https://doi.org/10.1186/cc11442.

[43] M. Jiménez-Alcázar, C. Rangaswamy, R. Panda, J. Bitterling, Y.J. Simsek, A. T. Long, R. Bilyy, V. Krenn, C. Renné, T. Renné, S. Kluge, U. Panzer, R. Mizuta, H. G. Mannherz, D. Kitamura, M. Herrmann, M. Napirei, T.A. Fuchs, Host DNases prevent vascular occlusion by neutrophil extracellular traps, Science 358 (2017) 1202–1206, https://doi.org/10.1126/science.aam8897.

[44] J.W. Black, A.F. Crowther, R.G. Shanks, L.H. Smith, A.C. Dornhorst, A new adrenergic betareceptor antagonist, Lancet 1 (1964) 1080–1081, https://doi.org/10.1016/s0140-6736(64)91275-9.

[45] O.J. Kennedy, M. Kicinski, S. Valpione, S. Gandini, S. Suciu, C.U. Blank, G.V. Long, V.G. Atkinson, S. Dalle, A.M. Haydon, A. Meshcheryakov, A. Khattak, M.S. Carlino, S. Sandhu, J. Larkin, S. Puig, P.A. Ascierto, P. Rutkowski, D. Schadendorf, R. Koornstra, L. Hernandez-Aya, A.M. Di Giacomo, A.J.M. van den Eertwegh, J. J. Grob, R. Gutzmer, R. Jamal, A.C.J. van Akkooi, C. Robert, A.M.M. Eggermont, P. Lorigan, M. Mandala, Prognostic and predictive value of β-blockers in the EORTC 1325/KEYNOTE-054 phase III trial of pembrolizumab versus placebo in resected high-risk stage III melanoma, Eur. J. Cancer 165 (2022) 97–112, https://doi.org/10.1016/j.ejca.2022.01.017.

[46] S. Zhou, J. Li, J. Yu, Y. Wang, Z. Wang, Z. He, D. Ouyang, H. Liu, Y. Wang, Tumor microenvironment adrenergic nerves blockade liposomes for cancer therapy, J. Contr. Release 351 (2022) 656–666, https://doi.org/10.1016/j.jconrel.2022.09.049.